

# BUNCHED BEAM ENVELOPE INSTABILITY IN A PERIODIC FOCUSING CHANNEL\*

J. Qiang<sup>†</sup>, LBNL, Berkeley, USA

## Abstract

The space-charge driven envelope instability presents a great danger in high intensity accelerator design. In this paper, we report on the study of bunched beam envelope instability in a periodic focusing channel using three-dimensional envelope model for a 3D uniform Waterbag distribution and a 3D Gaussian distribution. Our results show that the envelope instability stopband becomes broader with the increase of longitudinal focusing and are not sensitive to the type of distribution. Self-consistent macroparticle simulations using both distributions show similar structure in emittance growth but also extra instability stopbands. The emittance growth from the Waterbag distribution has larger stopband than that from the Gaussian distribution.

## INTRODUCTION

The space-charge driven envelope instability presents a potentially great danger in high intensity accelerators by causing beam size blow up and quality degradation. It has been studied theoretically [1–13] and experimentally [14–16] since 1980s. However, most of those theoretical studies were based on a two-dimensional model. Three-dimensional macroparticle simulations were carried out for a bunched beam under the guidance of the two-dimensional envelope instability model [10, 13]. Recently, 3D envelope instability analysis was done for a 3D ellipsoidal uniform Waterbag beam in periodic focusing channels using a 3D envelope equation model [17]. In this paper, we study the sensitivity of the instability stopband with another Gaussian distribution. We also compare the instability stopband from the envelope model with the emittance growth from the self-consistent macroparticle simulations.

## THREE-DIMENSIONAL ENVELOPE INSTABILITY ANALYSIS

For a 3D uniform density ellipsoidal beam inside a periodic focusing channel without acceleration, the three-dimensional envelope equations are given as [18–20]:

$$\frac{d^2 X}{ds^2} + k_x^2(s)X - I_x(X, Y, Z)X - \frac{\epsilon_x^2}{X^3} = 0 \quad (1)$$

$$\frac{d^2 Y}{ds^2} + k_y^2(s)Y - I_y(X, Y, Z)Y - \frac{\epsilon_y^2}{Y^3} = 0 \quad (2)$$

$$\frac{d^2 Z}{ds^2} + k_z^2(s)Z - I_z(X, Y, Z)Z - \frac{(\epsilon_z/\gamma^2)^2}{Z^3} = 0 \quad (3)$$

\* Work supported by the U.S. Department of Energy under Contract No. DE-AC02-05CH11231.

<sup>†</sup> jqiang@lbl.gov

with

$$I_i(X, Y, Z) = C \int_0^\infty \frac{dt}{(e_i^2 + t)\sqrt{(X^2 + t)(Y^2 + t)(\gamma^2 Z^2 + t)}} \quad (4)$$

where  $X$ ,  $Y$ , and  $Z$  are horizontal, vertical, and longitudinal rms beam sizes respectively,  $k_x^2$ ,  $k_y^2$ ,  $k_z^2$  represent the external periodic focusing forces  $\epsilon_x$ ,  $\epsilon_y$ , and  $\epsilon_z$  are unnormalized rms emittances,  $e_i = X, Y, \gamma Z$ , for  $i = x, y, z$ , and  $C = \frac{1}{2} \frac{3}{4\pi\epsilon_0} \frac{q}{mc^2} \frac{I}{f_{rf}\beta^2\gamma^2} \frac{1}{5\sqrt{5}}$ . Here,  $\epsilon_0$  is the vacuum permittivity,  $q$  the charge,  $mc^2$  the rest energy of the particle,  $c$  the light speed in vacuum,  $I$  the average beam current,  $f_{rf}$  the RF bunch frequency,  $\beta = v/c$ ,  $v$  the bunch velocity, and the relativistic factor  $\gamma = 1/\sqrt{1-\beta^2}$ . The nonlinear space-charge defocusing terms  $I_{x,y,z}$  depend on the horizontal, vertical, and longitudinal rms beam sizes and provide coupling between the transverse and longitudinal envelope oscillations. It was pointed out in reference [18] that the space-charge form factor  $1/5\sqrt{5}$  for a uniform distribution depends only weakly on the type of distributions and is  $1.01/5\sqrt{5}$  for a parabolic distribution and  $1.05/5\sqrt{5}$  for a Gaussian distribution. The external periodic focusing forces  $k_{x,y,z}(s) = k_{x,y,z}(s+L)$  in above equations vary for different accelerator beam line elements.

The above equations can be linearized with respect to periodic solutions (i.e. matched solutions) as:

$$X(s) = X_0(s) + x(s) \quad (5)$$

$$Y(s) = Y_0(s) + y(s) \quad (6)$$

$$Z(s) = Z_0(s) + z(s) \quad (7)$$

where  $X_0$ ,  $Y_0$  and  $Z_0$  denote the periodic matched envelope solutions and  $x$ ,  $y$  and  $z$  denote small perturbations

$$x(s) \ll X_0(s), \quad y(s) \ll Y_0(s), \quad z(s) \ll Z_0(s) \quad (8)$$

The equations of motion for these small perturbations are given by:

$$\frac{d^2 x}{ds^2} + a_1(s)x(s) + a_{12}(s)y(s) + \gamma^2 a_{13}(s)z(s) = 0 \quad (9)$$

$$\frac{d^2 y}{ds^2} + a_{12}(s)x(s) + a_2(s)y(s) + \gamma^2 a_{23}(s)z(s) = 0 \quad (10)$$

$$\frac{d^2 z}{ds^2} + a_{13}(s)x(s) + a_{23}(s)y(s) + a_3(s)z(s) = 0 \quad (11)$$

where

$$a_1(s) = k_x^2 + 3\epsilon_x^2/X_0^4 - I_x(X_0, Y_0, Z_0) + 3X_0^2 F_{xx} \quad (12)$$

$$a_{12}(s) = X_0 Y_0 F_{xy} \quad (13)$$

$$a_{13}(s) = X_0 Z_0 F_{xz} \quad (14)$$

$$a_2(s) = k_y^2 + 3\epsilon_y^2/Y_0^4 - I_y(X_0, Y_0, Z_0) + 3Y_0^2 F_{yy} \quad (15)$$

$$a_{23}(s) = Y_0 Z_0 F_{yz} \quad (16)$$

$$a_3(s) = k_z^2 + 3(\epsilon_z/\gamma^2)^2/Z_0^4 - I_z(X_0, Y_0, Z_0) + 3\gamma^2 Z_0^2 F_{zz} \quad (17)$$

Content from this work may be used under the terms of the CC BY 3.0 licence (© 2018). Any distribution of this work must maintain attribution to the author(s), title of the work, publisher, and DOI.

where

$$F_{xx} = C \int_0^\infty (X_0^2 + t)^{-5/2} (Y_0^2 + t)^{-1/2} (Z_0^2 \gamma^2 + t)^{-1/2} dt \quad (18)$$

$$F_{xy} = C \int_0^\infty (X_0^2 + t)^{-3/2} (Y_0^2 + t)^{-3/2} (Z_0^2 \gamma^2 + t)^{-1/2} dt \quad (19)$$

$$F_{xz} = C \int_0^\infty (X_0^2 + t)^{-3/2} (Y_0^2 + t)^{-1/2} (Z_0^2 \gamma^2 + t)^{-3/2} dt \quad (20)$$

$$F_{yy} = C \int_0^\infty (X_0^2 + t)^{-1/2} (Y_0^2 + t)^{-5/2} (Z_0^2 \gamma^2 + t)^{-1/2} dt \quad (21)$$

$$F_{yz} = C \int_0^\infty (X_0^2 + t)^{-1/2} (Y_0^2 + t)^{-3/2} (Z_0^2 \gamma^2 + t)^{-3/2} dt \quad (22)$$

$$F_{zz} = C \int_0^\infty (X_0^2 + t)^{-1/2} (Y_0^2 + t)^{-1/2} (Z_0^2 \gamma^2 + t)^{-5/2} dt \quad (23)$$

With  $\xi = (x, x', y, y', z, z')^T$ , the above equations can be rewritten in matrix notation as:

$$\frac{d\xi}{ds} = A_6(s)\xi(s) \quad (24)$$

with the periodic matrix

$$A_6(s) = \begin{pmatrix} 0 & 1 & 0 & 0 & 0 & 0 \\ -a_1(s) & 0 & -a_{12}(s) & 0 & -\gamma^2 a_{13}(s) & 0 \\ 0 & 0 & 0 & 1 & 0 & 0 \\ -a_{12}(s) & 0 & -a_2(s) & 0 & -\gamma^2 a_{23}(s) & 0 \\ 0 & 0 & 0 & 0 & 0 & 1 \\ -a_{13}(s) & 0 & -a_{23}(s) & 0 & -a_3(s) & 0 \end{pmatrix} \quad (25)$$

Let  $\xi(s) = M_6(s)\xi(0)$ , substituting this equation into Eq. 24 results in

$$\frac{dM_6(s)}{ds} = A_6(s)M_6(s) \quad (26)$$

where  $M_6(s)$  denotes the  $6 \times 6$  transfer matrix solution of  $\xi(s)$  and  $M_6(0)$  is a  $6 \times 6$  unit matrix. The above ordinary differential equation can be solved using the matched envelope solutions and numerical integration. The stability of these envelope perturbations is determined by the eigenvalues of the transfer matrix  $M_6(L)$  through one lattice period. For the envelope oscillation to be stable, all six eigenvalues (three pairs) of the  $M_6(L)$  have to stay on the unit circle. The amplitude of the eigenvalue gives the envelope mode growth (or damping) rate through one lattice period, while the phase of the eigenvalue yields the mode oscillation frequency. When the amplitude of any eigenvalue is greater than one, the envelope oscillation becomes unstable.

## ENVELOPE INSTABILITY IN A PERIODIC CHANNEL

We studied the envelope instability in a transverse solenoid focusing and longitudinal RF focusing periodic channel. A schematic plot of this periodic channel is shown in Fig. 1. Each period of the channel consists of a 0.1 meter solenoid, a 0.4 meter RF bunching cavity and two 0.1 meter drifts. The total length of the period is 0.7 meters. The proton bunch has a kinetic energy of 10 MeV and normalized

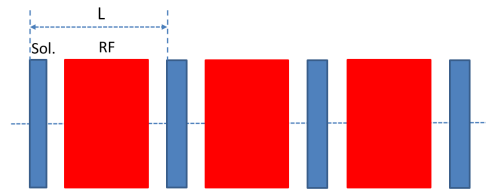


Figure 1: Schematic plot of a periodic solenoid and RF channel.

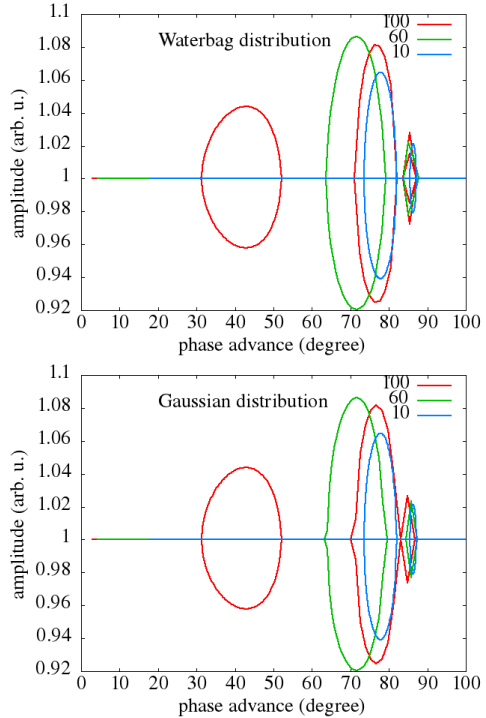


Figure 2: The 3D envelope mode growth rate amplitudes as a function of depressed transverse phase advance with 100 degree zero current transverse phase advances and 100 degree, 60 degree, and 10 degree zero current longitudinal phase advances in a periodic solenoid-RF channel using (top) 3D Waterbag uniform distribution and (bottom) 3D Gaussian distribution.

rms emittances of 0.2  $\mu\text{m}$ , 0.2  $\mu\text{m}$ , and 0.2  $\mu\text{m}$  in horizontal, vertical, and longitudinal directions respectively.

Figure 2 shows the 3D envelope mode growth rate amplitudes as a function of transverse depressed phase advance for 100 degree zero current transverse and 100, 60 and 10 degree longitudinal phase advances using the Waterbag distribution and the Gaussian distribution. It is seen that the instability stopbands are nearly the same for both distributions. For the zero current longitudinal phase advance below 90 degrees, the instability stopband width becomes broader with larger zero current longitudinal phase advance. When the zero current longitudinal phase advance attains 100 degrees, the instability structure becomes more complex and a new stopband appears below 50 degrees.

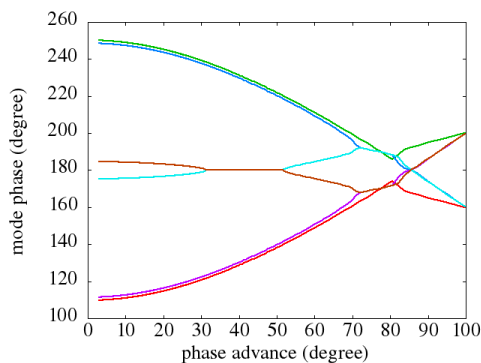


Figure 3: The 3D envelope mode phases as a function of depressed transverse phase advance with 100 degree zero current longitudinal and transverse phase advances in a periodic solenoid-RF channel using 3D Waterbag distribution. The six colors are the phases of the six eigenvalues.

Figure 3 shows the envelope eigenmode phases as a function of transverse depressed phase advance for the 100 degree zero current phase advance in both directions. It is seen that between 30 and 50 degree depressed phase advance, the eigenmode phases are locked at 180 degrees and the resultant instability is due to half-integer parametric resonance between the focusing lattice and the envelope oscillation mode. Between 70 and 85 degree phase advance, two eigenmodes attain the same phases and the resultant instability is called confluent resonance between two envelope modes since they have the same oscillation frequencies.

The instability stopbands from the 3D envelope analysis were compared with the emittance growth from self-consistent macroparticle simulations. Using above lattice setting and initial matched distribution, we carried out 3D macroparticle simulation using a parallel quasi-static particle-in-cell code, IMPACT. Figure 4 shows the maximum emittance growth within 200 lattice periods as a function of depressed transverse phase advance for the above case using both the 3D Waterbag uniform distribution and the 3D Gaussian distribution. Here, we have used 625664 macroparticles and  $64 \times 64 \times 64$  computational grid points in the simulations. It is seen that for both initial distributions, the emittance growth show similar structures to the envelope instability stopband. For the zero current longitudinal phase advance below 90 degrees, there exists major emittance growth between 70 and 80 degree depressed transverse phase advance. With 100 degree zero current longitudinal phase advance, the emittance growth structure becomes more complex as the envelope instability stopband does. Besides the stopband between the 70 and 80 degree phase advance, there is another stopband between 40 and 50 degrees. Moreover, self-consistent simulations show another emittance growth stopband between 30 and 40 degrees. This growth is probably due to strong tune depression and results in higher order collective mode instabilities that is not included in the rms envelope model. Comparing the emittance growth from the Waterbag distribution and the Gaussian

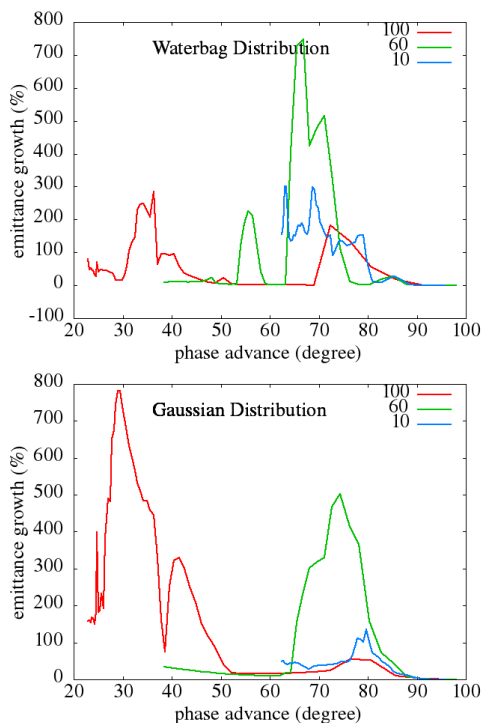


Figure 4: Maximum emittance growth within 200 lattice periods as a function of depressed transverse phase advance with 100 degree zero current transverse phase advances and 100 degree, 60 degree, and 10 degree zero current longitudinal phase advances in a periodic solenoid-RF channel using (top) 3D Waterbag distribution and (bottom) 3D Gaussian distribution.

distribution, we see some differences in emittance growth stopbands. For 60 degree zero current longitudinal phase advance, the Waterbag distribution shows an extra stopband between 50 and 60 degree depressed transverse phase advances. Such a stopband does not appear in the emittance growth from the initial Gaussian distribution. This is due to the long tail of the Gaussian distribution that provides the Landau damping to the instability. This instability stopband is not observed in the envelope instability stopband either and could result from the third order collective mode [1] that is absent in the rms envelope model. For 10 degree zero current phase advance, the Waterbag distribution shows a broader stopband width between 60 and 80 degree phase advance than the Gaussian distribution that has a longer tail and stronger damping effects. The emittance growth between 60 and 70 transverse depressed phase advance using the Waterbag distribution might be related to the third or fifth order collective modes, but needs to be further studied.

## ACKNOWLEDGMENT

We would like to thank Dr. R. D. Ryne for the use of his 3D envelope code. This research used computer resources at the National Energy Research Scientific Computing Center.

## REFERENCES

- [1] I. Hofmann, L. J. Laslett, L. Smith, and I. Haber, *Part. Accel.* 13, 145 (1983).
- [2] J. Struckmeier and M. Reiser, *Part. Accel.* 14, 227 (1984).
- [3] I. Hofmann, *Phys. Rev. E* 57, 4713 (1998).
- [4] R. C. Davidson, H. Qin, and G. Shvets, *Phys. Plasmas* 7, 1020 (2000).
- [5] H. Okamoto and K. Yokoya, *Nucl. Instrum. Methods Phys. Res., A* 482, 51 (2002).
- [6] A. V. Fedotov and I. Hofmann, *Phys. Rev. Spec. Top.-Accel. Beams* 5, 024202 (2002).
- [7] S. M. Lund and B. Bukh, *Phys. Rev. Spec. Top.-Accel. Beams* 7, 024801 (2004).
- [8] D. Jeon, L. Groening, and G. Franchetti, *Phys. Rev. Spec. Top.-Accel. Beams* 12, 054204 (2009).
- [9] C. Li and Y. L. Zhao, *Phys. Rev. ST Accel. Beams* 17, 124202 (2014).
- [10] I. Hofmann and O. Boine-Frankenheim, *Phys. Rev. Lett.* 115, 204802 (2015).
- [11] O. Boine-Frankenheim, I. Hofmann, and J. Struckmeier, *Phys. Plasmas* 23, 090705 (2016).
- [12] I. Hofmann and O. Boine-Frankenheim, *Phys. Rev. Lett.* 118, 114803, (2017).
- [13] I. Hofmann and O. Boine-Frankenheim, *Phys. Rev. Accel. Beams* 20, 014202 (2017).
- [14] M. Tiefenback, "Space charge limits on the transport of ion beams in a long alternating gradient system," Ph.D. thesis, Lawrence Berkeley National Laboratory Report LBL-22465, 1986.
- [15] E. P. Gilson, M. Chung, R. C. Davidson P. C. Efthimion, and R. Majeski, *Phys. Rev. Spec. Top.-Accel. Beams* 10, 124201 (2007).
- [16] L. Groening, W. Barth, W. Bayer, G. Clemente, L. Dahl, P. Forck, P. Gerhard, I. Hofmann, M. S. Kaiser, M. Maier, S. Mickat, and T. Milosic, *Phys. Rev. Lett.* 102, 234801 (2009).
- [17] J. Qiang, *Phys. Rev. Accel. Beams* 21, 034201 (2018).
- [18] F. J. Sacherer, *IEEE Trans. Nucl. Sci.* 18, 1101 (1971).
- [19] R. Ryne, Los Alamos Report No. LA-UR-95-391;; <http://xxx.lanl.gov/abs/acc-phys/9502001>
- [20] J. Qiang and R. D. Ryne, *Phys. Rev. ST Accel. Beams* 3, 064201 (2000).

Content from this work may be used under the terms of the CC BY 3.0 licence (© 2018). Any distribution of this work must maintain attribution to the author(s), title of the work, publisher, and DOI.